Virology 490 (2016) 49–58

Contents lists available at ScienceDirect

Virology

journal homepage: www.elsevier.com/locate/yviro

3B11-N, a monoclonal antibody against MERS-CoV, reduces lung pathology in rhesus monkeys following intratracheal inoculation of MERS-CoV Jordan-n3/2012

Reed F. Johnson [a,*], Ulas Bagci [b,h], Lauren Keith [c], Xianchun Tang [d], Daniel J. Mollura [b], Larry Zeitlin [e], Jing Qin [f], Louis Huzella [c], Christopher J. Bartos [c], Natasha Bohorova [e], Ognian Bohorov [e], Charles Goodman [e], Do H. Kim [e], Michael H. Paulty [e], Jesus Velasco [e], Kevin J. Whaley [e], Joshua C. Johnson [c], James Pettitt [c], Britini L. Ork [c], Jeffrey Solomon [i], Nicholas Oberlander [c], Quan Zhu [d], Jiusong Sun [d], Michael R. Holbrook [c], Gene G. Olinger [c], Ralph S. Baric [g], Lisa E. Hensley [c], Peter B. Jahrling [a,c], Wayne A. Marasco [d]

[a] Emerging Viral Pathogens Section National Institute of Allergy and Infectious Diseases, National Institutes of Health, Frederick, MD 21702, USA
[b] Center for Infectious Disease Imaging, National Institutes of Health Clinical Center, Bethesda MD 20892, USA
[c] Integrated Research Facility, National Institute of Allergy and Infectious Diseases, National Institutes of Health, Frederick, MD 21702, USA
[d] Department of Cancer Immunology & AIDS, Dana-Farber Cancer Institute, Harvard Medical School, Boston, MA 02215, USA
[e] Mapp Biopharmaceutical, Inc., San Diego CA 92121, USA
[f] Biostatistics Research Branch, National Institute of Allergy and Infectious Diseases, National Institutes of Health, Bethesda, MD 20892, USA
[g] Department of Microbiology and Immunology, Department of Epidemiology, University of North Carolina at Chapel Hill, Chapel Hill, NC 27599, USA
[h] Center for Research in Computer Vision (CRCV), Department of Electrics Electronics and Computer Science, University of Central Florida, Orlando, FL 32816, USA.
[i] Clinical Research Directorate/Clinical Monitoring Research Program, Leidos Biomedical Research, Inc., Frederick National Laboratory for Cancer Research, Frederick, MD 21702-USA.

ARTICLE INFO

Article history:
Received 14 December 2015
Returned to author for revisions
4 January 2016
Accepted 11 January 2016
Available online 30 January 2016

Keywords:
MERS-CoV
Antibody therapy
Animal model, MERS
Respiratory syndrome
Human monoclonal antibody therapy

ABSTRACT

Middle East Respiratory Syndrome Coronavirus (MERS-CoV) was identified in 2012 as the causative agent of a severe, lethal respiratory disease occurring across several countries in the Middle East. To date there have been over 1600 laboratory confirmed cases of MERS-CoV in 26 countries with a case fatality rate of 36%. Given the endemic region, it is possible that MERS-CoV could spread during the annual Hajj pilgrimage, necessitating countermeasure development. In this report, we describe the clinical and radiographic changes of rhesus monkeys following infection with 5×10^6 PFU MERS-CoV Jordan-n3/2012. Two groups of NHPs were treated with either a human anti-MERS monoclonal antibody 3B11-N or E410-N, an anti-HIV antibody. MERS-CoV Jordan-n3/2012 infection resulted in quantifiable changes by computed tomography, but limited other clinical signs of disease. 3B11-N treated subjects developed significantly reduced lung pathology when compared to infected, untreated subjects, indicating that this antibody may be a suitable MERS-CoV treatment.

Published by Elsevier Inc.

Introduction

In September of 2012, a novel coronavirus was discovered in a patient suffering from a severe acute respiratory disease termed Middle East Respiratory Syndrome (MERS) (Zaki et al., 2012), subsequently the virus was renamed MERS-CoV (de Groot et al., 2013). Thus far, 26 nations have reported over 1600 MERS cases with a case fatality rate of 36% (http://www.who.int/emergencies/mers-cov/en/). Fortunately, MERS-CoV has yet to demonstrate sustained human to human transmission. However, given the estimated 2.5 million pilgrims to the MERS-CoV endemic region for the Hajj, MERS-CoV represents a continued global health risk. Despite a substantial response by health agencies, MERS-CoV infections continue and have spread geographically due to travel as evidenced by the recent outbreak in the Republic of Korea (186 cases with 36 deaths), and single cases in Thailand, Philippines, and China (http://www.who.int/emergencies/mers-cov/mers-cov-republic-of-korea-and-china-risk-assessment-19-june-2015.pdf?ua=1). Unfortunately, the definitive reservoir has yet to be

* Corresponding author.
E-mail address: johnsonreed@mail.nih.gov (R.F. Johnson).

http://dx.doi.org/10.1016/j.virol.2016.01.004
0042-6822/Published by Elsevier Inc.

identified, although camels are heavily implicated and may at least serve as an intermediate host. If so, then camels may provide an intervention point to prevent human disease (Adney et al., 2014; Gossner et al., 2014; Khalafalla et al., 2015; Yusof et al., 2015). If MERS-CoV was able to establish efficient human to human transmission and maintain pathogenicity, then the increased number of patients and the special care they require could rapidly place a strain on healthcare resources. Treatment thus far has been supportive with reports of patients placed on extracorporeal membrane oxygenation, commonly known as ECMO, to maintain their health (Pebody et al., 2012). To date, no MERS-CoV-specific countermeasures or treatment programs have been developed.

MERS countermeasure development depends on appropriate animal models. An ideal laboratory animal model would uniformly recapitulate the most severe outcome of human disease. To date, three murine models have been reported that express the MERS-CoV receptor, human dipeptidyl peptidase 4 (DPP4 or CD26) in the respiratory track through adenovirus transduction of the airway (Zhao et al., 2014) or construction of transgenic or humanized mice through genomics techniques (Agrawal et al., 2015; Pascal et al., 2015). These mouse models serve complementary roles in the evaluation of medical countermeasures (Channappanavar et al., 2014a, 2014b), MERS-CoV respiratory disease (Agrawal et al., 2015) and lung pathology (Pascal et al., 2015). Common marmosets (*Callithrix jacchus*) have also been evaluated as a MERS model (Falzarano et al., 2014; Johnson et al., 2015). They develop limited disease as shown by histopathological analysis, radiological analysis, and qRT-PCR evidence of virus replication in the lung, but do not develop a severe respiratory disease that faithfully replicates the human condition.

A nonhuman primate model is an important part of any drug discovery process because of the close phylogenetic relatedness to humans and their use in being granted regulatory approval to move into human clinical trials. The nonhuman primate (NHP) (*Macaca mulatta*) model of MERS has been described by two groups (de Wit et al., 2013; Yao et al., 2014). In this model, exposure of rhesus monkeys to MERS-CoV leads to a transient lung infection that results in variable lung pathology consisting of inflammatory infiltrates as well as transient radiological lung findings. However, to date, there are no reports of using this model to evaluate a new anti-MERS drug. There is renewed interest in the use of monoclonal antibodies to treat viral infections (reviewed in (Bossart et al., 2009; Marasco and Sui, 2007; Qiu and Kobinger, 2014; Shadman and Wald, 2011). We and others have identified neutralizing antibodies against MERS-CoV (Jiang et al., 2014; Tang et al., 2014; Ying et al., 2015). In this study we describe intratracheal inoculation of rhesus monkeys with MERS-CoV Jordan-n3/2012 as well as a pilot study demonstrating efficacy of 3B11-N, a human monoclonal antibody against MERS-CoV spike protein to reduce lung pathology following MERS-CoV infection.

Results

Experimental design

The experiment was performed in two parts. The initial part was establishment of the rhesus MERS-CoV infection model using MERS-CoV Jordan-n3/2012 (MERS-JOR). The second part was evaluation of the anti-MERS-CoV monoclonal antibody 3B11-N. In total, five groups of NHPs were evaluated as shown in Fig. 1. Computed Tomography (CT) was chosen over standard radiography because 1) CT is quantifiable, which allows for direct comparisons between groups with reduced bias, and 2) CT provides a 3-dimensional representation of the region of interest whereas standard radiography compresses 3-dimensional images into 2 dimensions and may misrepresent

	Study days	Group 1 (Mock) CT	Group 1 (Mock) Blood draw	Group 2 (Virus only) CT	Group 2 (Virus only) Blood draw	Group 3 (Virus + BAL) CT	Group 3 (Virus + BAL) Blood draw	Group 4 (Anti-MERS mAb) CT	Group 4 (Anti-MERS mAb) Blood draw	Group 5 (Control mAb) CT	Group 5 (Control mAb) Blood draw
	BL 1	N=1	N=2	N=1	N=2	N=1	N=1	N=3	N=3	N=3	N=3
	BL 2	N=1		N=1				N=3		N=3	
	BL 3	N=2		N=2							
Challenge →	0				N=2	N=1	N=1				
	1	N=2	N=2	N=1	N=1	N=1	N=1	N=3		N=3	
	2			N=2	N=1	N=2	N=1				
	3	N=2	N=2		N=1	N=1	N=1	N=3		N=3	
	4			N=1	N=1		N=1				
	5	N=2	N=2	N=1	N=1	N=1	N=1	N=3		N=3	
	6			N=1	N=1	N=1	N=1				
	7	N=2	N=2	N=1		N=1		N=3	N=3	N=3	N=3
	8			N=1	N=1	N=1	N=1				
	9	N=2	N=2	N=2	N=2	N=2	N=2				
	10			N=1	N=1		N=1				
	11							N=3	N=3	N=3	N=3
	13	N=2	N=2	N=1	N=1	N=1	N=1				
	14			N=1	N=1		N=1				
	22	N=2	N=2								
Challenge →	26				N=1		N=1				
	27			N=1	N=1		N=1				
	29				N=1						
	30			N=2	N=1	N=2	N=1				
	31			N=1		N=1					
	32				N=1	N=1					
	33							N=3	N=3	N=3	N=3
	43			N=1	N=1	N=1					
	44			N=1	N=1		N=1				
Challenge →	88				N=2		N=2				
	89			N=2	N=2	N=2	N=2				
	91			N=2	N=2		N=2				
	93			N=1	N=1		N=1				

Fig. 1. 5 Groups of rhesus monkeys were challenged by IT infection with 5×10^6 PFU of MERS-JOR or γ-irradiated virus as shown. Periodic CT and blood draws were performed; *N* represents the number of subjects from each group that underwent the indicated procedures. The variation in number of procedures performed on a given day was logistically determined based on blood withdrawal limits and accessibility to the CT, Each subject was given a complete physical exam prior to CT or blood withdrawal.

pathology. In this study, two subjects (Group 1) were inoculated with γ-irradiated 5×10^6 PFU MERS-JOR and received periodic bronchoalveolar lavage (BAL) to determine the impact of the infection procedures and viral antigens would have on lung pathology as measured by CT. Group 2 consisted of two subjects that received 5×10^6 PFU MERS-JOR by intratracheal (IT) inoculation without BAL to determine the impact of virus on lung pathology and two subjects (Group 3) that received 5×10^6 PFU of infectious MERS-JOR with periodic BAL to determine the impact of BAL on the observed lung pathology. Group 2 and 3 subjects were re-challenged at days 26 and 88 to determine if there was immune enhanced disease and to match pathology findings with radiology findings; BALs were also performed on Group 3 subjects following re-challenge. Group 4 consisted of three subjects that received 5×10^6 PFU of infectious virus by IT inoculation preceded by treatment with 311B-N 1 day prior to infection. Finally, Group 5 was comprised of 3 subjects that received 5×10^6 PFU of infectious virus by IT inoculation preceded by treatment with an antibody against HIV-1 (4E10-N, (Zwick et al., 2001)) 1 day prior to infection as a non-specific control antibody.

MERS-JOR infected rhesus do not develop clinical signs of disease

Physical examination and daily observations indicate that MERS-CoV infected rhesus did not develop obvious clinical signs of MERS. Body temperature was measured rectally and was within the normal range for rhesus monkeys (Fig. 2A). Peripheral oxygen saturation, a measure of respiratory function, did not decrease below normal values (Fig. 2A). Signs of respiratory disease such as tussis and dyspnea were not observed. Although mild, increases in

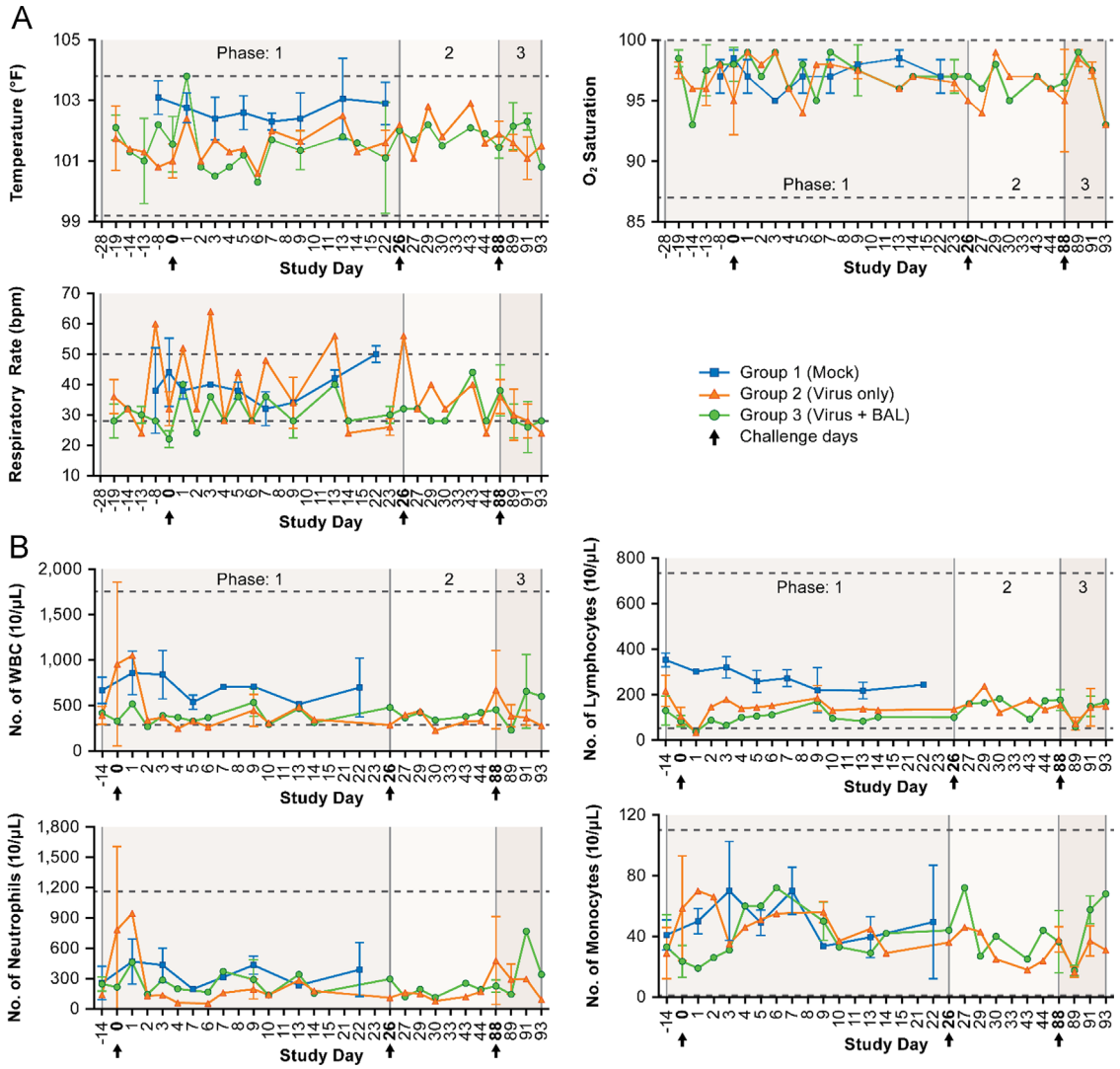

Fig. 2. Rhesus monkeys demonstrated limited clinical indicators of disease in response to infection with MERS-CoV Jordan-n3/2012. (A) Temperature, respiratory rate and peripheral oxygen saturation were within normal ranges for rhesus monkeys. (B) CBC/Diff data indicating limited response to MERS-CoV inoculation. WBC, lymphocyte, neutrophil and monocyte total counts were within normal ranges, although some changes are observed. Hashed lines indicate normal value ranges. Group 1 Mock (blue squares), Group 2 5×10^6 PFU (orange triangles), and Group 3, Green circles (5×10^6 PFU w/BAL). Arrows indicate challenge and re-challenge days. The shaded backgrounds represent the different phases of the experiment, initial challenge, followed by the 2nd and 3rd challenges. (For interpretation of the references to color in this figure legend, the reader is referred to the web version of this article.)

respiratory rate were sporadically observed for the Group 2 subjects (Fig. 2A). The data indicates that MERS-JOR infection did not adversely impact lung function.

Complete blood count with differential (CBC/Diff) reinforced the physical examination data and no clinically significant changes were observed (Fig. 2B). A slight lymphopenia could be observed for Groups 2 and 3, 1 day post-infection, a slight neutropenia between days 2 and 6 post-infection for Groups 2 and 3, and a mild leukopenia between days 2 and 9 post-infection. CBC/Diff of the Groups 2 and 3 following re-challenges were comparable to the initial 2–9 day post–infection period. These data suggest that overt immune enhanced disease did not occur in these MERS-JOR infected rhesus monkeys.

qRT-PCR of whole blood, nasal swabs, and BAL samples were performed to determine viral load and dissemination from the site of infection. qRT-PCR results were below the limit of detection on all days across all groups in these samples indicating that there was no detectable dissemination of MERS-CoV from the lung to peripheral organs and limited virus replication. To obtain data at the acute phase of disease progression, subjects from Groups 2 and 3 were challenged a third time on study day 88 and one subject each from Groups 2 and 3 were necropsied on days 91 and 93 post-infection. Plaque assay of lung, liver, and kidney homogenate were negative as was serial passage of the tissue homogenate on MRC-5 cells, suggesting that MERS-JOR replication is restricted in these tissues.

Computed tomography indicates mild respiratory disease

To evaluate changes in lung architecture as a result of MERS-JOR infection, visual and quantitative analyses were performed. Briefly, lung volumes of interest were automatically extracted and quantified using a pathological lung delineation algorithm with high sensitivity and specificity (Mansoor et al., 2014). This procedure was followed by a statistical machine-learning scheme, called random forest classification, for pathological tissue identification and tissue morphology quantification including volume and density properties. The total

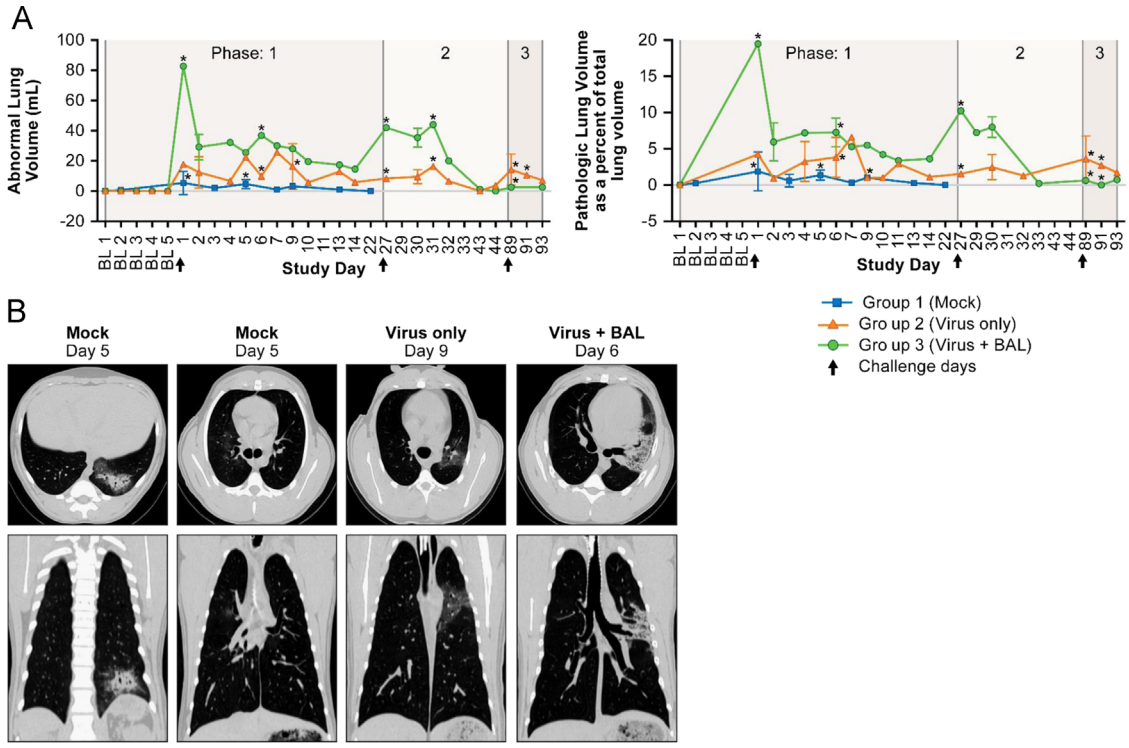

Fig. 3. MERS-CoV exposure of rhesus results in mild, but quantifiable lung pathology. (A) Lung volume quantification indicates mild, virus specific changes. Left panel is the total abnormal lung volume as quantified from CT data for Groups 1, 2, and 3. The data demonstrate that lung pathology is transient and re-challenge does not result in increased lung pathology. Right panel is the quantification of the CT as a percentage of total lung volume. Asterisks indicate days at which peak lung pathology was observed for individual subjects Group 1 Mock (blue squares), Group 2 5×10^6 PFU (orange triangles), and Group 3, 5×10^6 PFU w/BAL (green circles) Arrows indicate challenge and re-challenge days. The shaded backgrounds represent the different phases of the experiment, initial challenge, followed by the 2nd and 3rd challenges. (B) Representative CT of selected subjects from each group demonstrating peak lung pathology. (For interpretation of the references to color in this figure legend, the reader is referred to the web version of this article.)

lung capacity was refined by adding pathological tissues into the lung regions of interest (ROIs) and pathology percentage was computed using total lung capacity as a disease severity index. Averages of these values were compared between the groups (Fig. 3A). To adjust for the differences in total lung volume between the subjects the percent of pathologic lung volume was also calculated (Fig. 3A). These data also support a mild respiratory disease. CT abnormalities are shown at the peak value for the most effected member of each group and demonstrates the differences in observed lung pathology across the groups (Fig. 3B).

The two subjects in Group 1, and one or two subjects each from Group 2 and Group 3 was imaged per day on the schedule shown in Fig. 1. The peak observed lung pathology for subjects within each group were averaged from their peak responses for the initial 14 days following challenge. CT quantification indicated that peak lung pathology was observed for Group 1 at an average of 3 days post-infection (St. Dev 2.82). Group 2 peak lung pathology was observed at an average day 7.5 (St. Dev. 2.12) and an average of day 3.5 (St. Dev 3.5) for Group 3. Mean peak percentage of abnormal lung volume for Group 1 was 1.89% (St. Dev 1.36), Group 2 was 6.59% (St. Dev 3.3%, and Group 3 19.8% (St Dev. 6.54)). These data suggest that 1) the inoculation procedures can result in lung pathology, 2) MERS-JOR infection results in limited virus specific disease and 3) that BAL may exacerbate lung pathology.

For Groups 2 and 3 that were re-challenged on days 26 and 88 post-inoculation, a similar pattern of increased abnormal lung volume occurring 1–6 days post-infection following re-challenge on day 26. Similar to the initial challenge, subjects did not develop increased lung disease when compared to the initial infection which suggests that immune-enhanced disease did not occur in this experiment. Following the second infection, serial CTs indicated that the average peak percentage of abnormal lung volume was 2.64% (St. Dev 1.54) that occurred on average day 2 (St. Dev 2.83) post-second infection for Group 2 subjects and 9.6% (St. Dev 0.85) which also occurred 2 days (St. Dev 2.83) post-second infection for Group 3 subjects. Following the 3rd infection, 88 days after the initial infection, the peak lung pathology occurred on average 2 days (St. Dev 1.4) post-infection with an average abnormal lung volume percentage of 4.1% (St. Dev 2.53) for Group 2 and an average of 1 day post-infection with an average abnormal lung volume of 0.6% (St. Dev 0.2) for Group 3 (Fig. 3A).

MERS-CoV specific antibody treatment reduces lung pathology

In the first part of the experiment, we demonstrated that MERS-JOR exposure results in quantifiable lung pathology, therefore, we sought to determine the efficacy of a human anti-MERS-CoV monoclonal antibody, 311B-N. Groups 4 and 5 were treated with 311B-N or 4E10-N (an anti-HIV antibody), respectively, 1 day prior to infection. The subjects were given periodic physical exams, blood draws and CT's to monitor disease progression and 311B-N's potential efficacy (Supplemental Fig. 1). Representative CT's are shown in Fig. 4A. Quantification of the serial CT indicated that 311B-N treatment resulted in reduced lung pathology when compared to the control antibody (Fig. 4B). Pathologic lung volume for Group 4, 311B-N treated, peaked on average day 5 post-infection (St. Dev 1.4) with an average abnormal lung volume percentage of 0.9% (St. Dev 1.0) with one of 3 subjects demonstrating no abnormal lung volume. Group 5 subjects demonstrated a peak increase in abnormal lung volume percentage 7 days post-infection for all 3 subjects with an average of 4.3% (St Dev 3.86) of abnormal lung volume. These data support the conclusion that

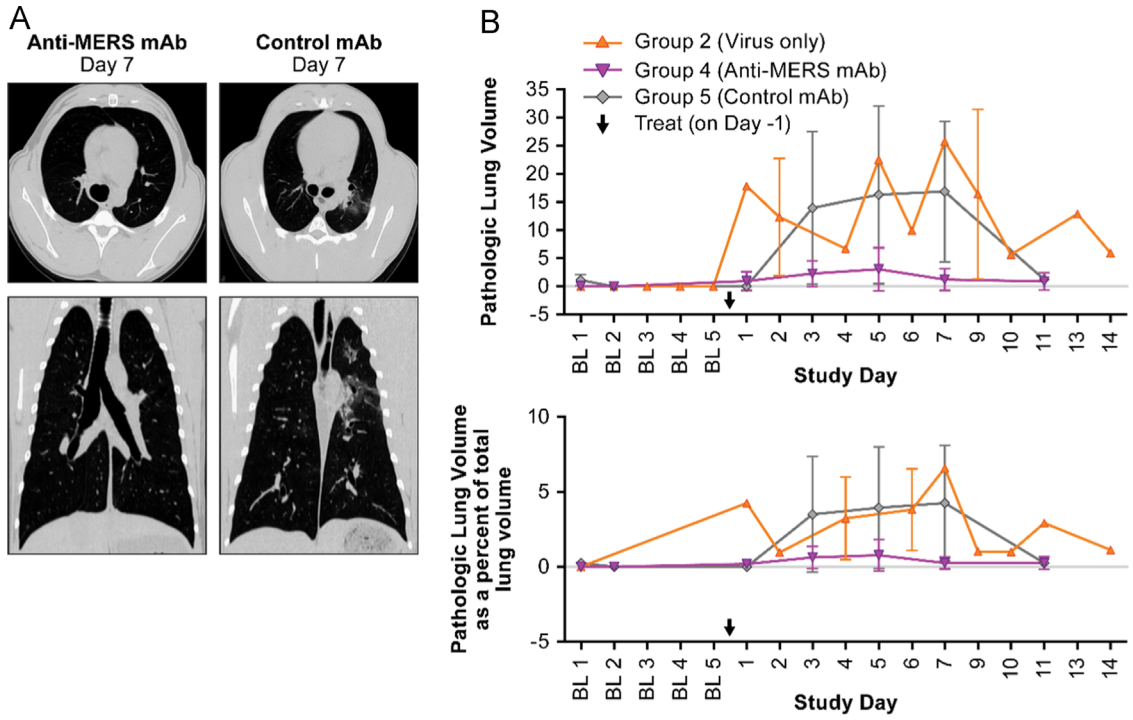

C

	Group 1 (Mock)	Group 2 (Virus only)	Group 3 (Virus + BAL)	Group 4 (Anti-MERS mAb)
Group 1 (Mock)	–			
Group 2 (Virus only)	-9.39 ± 4.0 *p* = 0.051	–		
Group 3 (Virus + BAL)	**-24.3 ± 4.0** ***p* = 0.0005**	**14.9 ± 4.0** ***p* = 0.007**	–	
Group 4 (Anti-MERS mAb)	1.48 ± 3.75 *p* = 0.71	**-10.87 ± 3.76** ***p* = 0.023**	**-25.77 ± 3.76** ***p* = 0.0002**	–
Group 5 (Control mAb)	-0.94 ± 3.75 *p* = 0.81	-8.45 ± 3.76 *p* = 0.06	**23.35 ± 3.76** ***p* = 0.004**	-2.42 ± 3.45 *p* = 0.51

Fig. 4. (A) Representative CT of selected subjects from each group demonstrating peak lung pathology. (B) Comparison between 3B11-N (Group 4, purple inverted triangle) and 4E10-N (Group 5, gray diamond). Treatment with 3B11-N resulted in statistically significantly ($p < 0.0001$) decreased lung pathology when compared to the untreated, infected group. Untreated, infected subjects (Group 2, orange triangle) were included for comparison. (C) Statistical comparisons between all groups which supports that BAL exacerbates disease. Days 0–14 for each group were analyzed by a linear mixed model. The summarized mean difference, standard error and *P* value are given in the table below. A *P* value of 0.01 was used to provide a stringent basis for significance. Comparisons with statistically significant differences are in bold. (For interpretation of the references to color in this figure legend, the reader is referred to the web version of this article.)

pre-treatment with MERS-CoV specific monoclonal antibody inhibited MERS-JOR induced lung pathology in this model. Comparison between the antibody treated groups by an unpaired, two-tailed t-test using GraphPad Prism indicated no significant difference ($p=0.1122$) between 311B-N and 4E10-N. Comparison of 311B-N treated subjects to untreated, MERS-CoV infected subjects by unpaired, two-tailed *t*-test using Graphpad Prism indicated a significant difference in observed lung pathology ($p < 0.0001$) when evaluated based on pathologic lung volume (Fig. 4B). When the diseased lung volume is calculated as a percentage of the total lung volume (Fig. 4B) a similar pattern is observed, no statistically significant difference was observed between the antibody treatments was found ($p=0.0877$). However, a significant difference was observed between 311B-N treated group (Group 4) and the infected, untreated subjects (Group 2) ($p=0.0017$) by unpaired, two-tailed *t*-test using Graphpad Prism 6.0. A statistical difference between these groups was also supported by linear mixed model analysis $p=0.023$ (Fig. 4C).

Statistical analysis indicates that BAL may exacerbate lung pathology

Because the experiments were performed in separate stages, statistical analysis using a linear mixed model was used to evaluate the abnormal lung volume measurements (Laird and Ware, 1982) and are shown in Fig. 4C. Statistically significantly differences were observed between Groups 1 and 3 ($p=0.0005$), Groups 2 and 3 ($p=0.007$), Groups 3 and 4 ($p=0.0002$), and Groups 3 and 5 ($p=0.004$). The statistical significance between Group 3 and the other groups indicates that BALs may exacerbate lung pathology and the impact of BAL must be accounted for in respiratory disease models. The lowest observed *p*-value ($p=0.0002$) for the comparison between Groups 3 and 4 suggests that the MERS-CoV antibody does inhibit development of abnormal lung pathology. No statistically significant difference was established between Group 4 and Group 1 ($p=0.71$), Group 4 and Group 5 ($p=0.051$), but a significant difference between Group 4 and Group 2 ($p=0.023$) was observed.

Pathological findings

Group 1 subjects were not euthanized and Group 4 and 5 subjects were euthanized between days 153–155 post-infection and no significant pathological changes were observed in these groups. For groups 2 and 3 CT data indicated medial lung pathology that may have followed the track of inoculum deposition therefore lung lobes were histologically evaluated individually. Histopathological results are summarized in Table 1. Histological examination of the lung revealed multifocal interstitial lymphohistocytic infiltrates, pulmonary congestion, and pulmonary edema with some epithelial cell degeneration.

Grossly, no major differences were observed between the day 91 and day 93 necropsied subjects. All 4 subjects' demonstrated diffuse pulmonary congestion of varying degree, 3 of 4 demonstrated tracheobronchial lymph node enlargement. One subject from Group 3 had hepatic discoloration and this subject was retrospectively diagnosed with amyloidosis. No signal of MERS-CoV antigen was detected by immunohistochemistry in select lung samples examined. BAL samples were evaluated histologically and contained predominantly alveolar macrophages (approx. 14–16 μm in diameter), many with pseudopodia, with few lymphocytes, red blood cells and few ciliated respiratory epithelial cells on background of proteinaceous/mucinous material with small amounts of surfactant and cellular debris. There were no clinically significant pathogens seen in lung examined under EM.

Table 1
Summary of histopathological examination of lymphoid and lung tissue.

	Severity: 0 (none), 1 (minimal), 2 (mild), 3 (moderate)			
	Group 2		Group 3	
	Incidence	Severity	Incidence	Severity
Spleen				
Lymphoid depletion	1	1	2	1,2
Hyalinization	1	2	0	0
Amyloid	1	3	0	0
Axillary lymph node				
Lymphoid depletion	2	1,1	2	1,2
Edema	0	0	0	0
Histiocytosis	2	1,2	2	1,2
Congestion	0	0	1	1
Mesenteric lymph node				
Lymphoid depletion	1	2	2	1,1
Edema	2	2,2	1	2
Histiocytosis	1	2	2	3,3
Congestion	0	0	0	0
Tracheobronchial lymph node				
Lymphoid depletion	0	0	0	0
Edema	2	2,2	1	2
Histiocytosis	2	2,2	2	2,2
Congestion	0	0	0	0
Mandibular lymph node				
Lymphoid depletion	1	1	0	0
Edema	0	0	2	1,1
Histiocytosis	0	0	2	1,1
Congestion	N/A		0	0
Right cranial lung				
Inflammation (lymphocytic/lymphohistiocytic)	1	2	1	1
Neutrophilic inflammation	0	0	0	0
Pulmonary congestion	2	2,2	2	1,3
Edema	2	2,2	2	1,3
Epithelial degeneration	2	2,2	0	0
Right medial lung				
Inflammation (lymphocytic/lymphohistiocytic)	2	2,2	1	0,2
Neutrophilic inflammation	1	2	1	3
Pulmonary congestion	1	2	1	1
Edema	1	2	2	3,1
Epithelial degeneration	2	2,3	2	2,3
Right caudal lung				
Inflammation (lymphocytic/lymphohistiocytic)	2	1,2	2	2,2
Neutrophilic inflammation	0	0	0	0
Pulmonary congestion	1	2	2	2,2
Edema	2	2,2	1	2
Epithelial degeneration	2	2,2	2	3,2
Left cranial lung				
Inflammation (lymphocytic/lymphohistiocytic)	2	2,3	2	2,2
Neutrophilic inflammation	0	0	0	0
Pulmonary congestion	2	2,2	2	1,2
Edema	2	2,2	1	3
Epithelial degeneration	2	2,2	2	2,2
Left caudal lung				
Inflammation lymphocytic/lymphohistiocytic	2	2,3	2	1,3
Neutrophilic inflammation	0	0	0	0
Pulmonary congestion	2	1,1	1	1
Edema	1	1	2	2,2
Epithelial degeneration	2	2,2	2	3,2

Discussion

The goal of this experiment was to establish the rhesus model of MERS in our laboratory and determine the efficacy of 3B11-N, a human monoclonal antibody against MERS-CoV. In our experiment, NHPs developed limited clinical signs of disease, but did develop quantifiable virus-induced changes in lung architecture following IT exposure of rhesus monkeys with MERS-JOR. We also demonstrate that the 3B11-N monoclonal antibody against MERS-CoV significantly reduces virus-induced lung pathology as measured by CT when compared to untreated subjects, thus warranting further investigation as a potential MERS-CoV countermeasure. The present study varies from previous studies of MERS-CoV in rhesus monkey due to 1) the use of MERS-JOR, 2) CT for evaluating structural changes in the lung, 3) comparison of subjects that received BAL and those that did not, 4) subjects were not euthanized at early timepoints post-infection to evaluate pathology and viral loads, and 5) subjects were re-challenged to determine if immune enhanced infection may occur. MERS-JOR infection of rhesus has not been previously described and the differences observed between our study and Munster and Yao's (Munster et al., 2013; Yao et al., 2014) indicated that other MERS-CoV isolates should be evaluated to determine if an improved model could be developed.

Overall, MERS-JOR inoculation of rhesus monkeys results in a mild disease. Our results in conjunction with (Munster et al. (2013) and Yao et al. (2014)) MERS-CoV EMC rhesus monkey experiments demonstrate mild disease with no striking clinical features, this lack of overt clinical signs limits the utility of the MERS-rhesus monkey model. However, medical imaging such as standard radiography and CT may provide alternate biomarkers of disease. Munster et al. (2013), de Wit et al. (2013) and Yao et al. (2014) also reported structural changes to the lung using standard radiography. However, standard radiography is limited because it does not provide a 3-dimensional view of the region of interest and subject to interpretation biases. An improvement on standard radiography is use of CT, which provides a quantifiable measure of pathology which can be standardized between studies, depending upon available equipment.

In this study, MERS-CoV induced disease progression and regression was measured by CT and subjects developed lung pathology that could be observed up to 22 days post-infection, but peaked between days 3 and 7 post-infection and followed a similar pattern after subsequent re-challenge in Group 2 and 3 subjects. A difference between Group 2 and Group 3 animals was

observed and is likely due to continued BAL procedures that were performed on Group 3 subjects. Furthermore, the comparison of Group 3 subjects to the other groups suggest that procedures such as BAL likely induce increased lung pathology that may confound study results, which has been described previously (Haley et al., 1989; Von Essen et al., 1991). de Wit et al. performed BAL on days 1, 3, and 6 post-infection and Yao et al. did not perform BAL and less respiratory disease was observed by radiography by Yao et al., supporting our findings that BAL does influence radiological findings. However, such a cross-laboratory comparison is difficult due to differences in methodology, available equipment, and inherent variability in interpretation of radiograms.

3B11-N was chosen based on initial characterization of the antibody in which no escape mutants were isolated, highest virus neutralizing ability, and the ability to produce large quantities. We have demonstrated that pre-treatment with a monoclonal antibody against the MERS-CoV spike protein significantly reduced severity of lung pathology when compared to untreated subjects. Lung pathology in 3B11-N treated subjects was roughly 10% of that in control antibody treated subjects and roughly equal to subjects that received γ-irradiated virus and BAL (Group 1). The lack of statistical significance between the control antibody and 3B11-N is likely due to the small and variable volume of lung pathology induced by MERS-CoV and the small group size ($n=3$). The p-value of the comparison between 3B11-N to 4E10-N treatments nearly reached significance ($p=0.051$) which further supports that larger group sizes may provide statistically significant differences. This pilot study paves the way for experiments utilizing larger group sizes with varying treatment strategies to include post exposure treatment and "trigger to treat" based on CT findings. Such experiments would also need to include control groups of "media only" and γ-irradiated virus to account for the possibility that γ-irradiated virus may also induce an inflammatory response.

We must note that two subjects were of advanced age and were assigned to Groups 4 (15 years old) and 5 (19 years old). The aged subject from Group 5 did demonstrate roughly three times the elevated abnormal lung pathology (34 ml, 8.6% of total lung volume) when compared to the other two subjects in the group (10 mL average, 2% of total lung volume), through the course of this study, this subject was diagnosed with diabetes. Although speculative, this finding supports human clinical observations that comorbidities such as diabetes may increase disease severity in humans. Further development of this potential anti-MERS-CoV treatment in NHP models would also involve potential use of subjects with comorbidities.

Similar findings to Munster's laboratory and Yao et al. include: transient respiratory disease that is primarily medial, lack of sustained fever development, mild changes in white blood cell counts, limited changes in peripheral oxygen saturation, and inflammatory infiltrates in the lungs (Munster et al. 2013; de Wit et al. 2013; Yao et al, 2014). Our findings contrast with the previously published results in that viral RNA and infectious virus could not be detected in BAL, lung, nasal, or oral swabs by qRT-PCR. Attempts to isolate infectious virus and qRT-PCR data indicate that virus replication is limited following MERS-JOR infection, which may be due to differences between rhesus DPP4/CD26 and human DPP4/CD26, the receptor for MERS-CoV (Raj et al., 2013).

MERS-CoV infections have steadily continued since its identification and the region most affected continues to be the Middle East, but the recent outbreak in the Republic of Korea reinforces the need for continued monitoring of MERS-CoV, development of countermeasures and a greater understanding of viral pathogenesis. Animal models that faithfully mimic human disease need to be developed for identification and evaluation of potential countermeasures as well as understanding disease processes. Rhesus monkeys and marmosets do not develop the severe disease that is observed in humans (Munster et al. 2013; Yao et al., 2014; Falzarano et al., 2014; Johnson et al., 2015), but to date are the available nonhuman primate models. Small animal models, particularly mice, have been explored as well. These models provide greater accessibility than NHP models and the availability of knockout mice, transgenic mice, and transduction models provide opportunities to study specific disease processes. Thus far, the two most commonly studied isolates are MERS-EMC and MERS-JOR. Other isolates should be evaluated in the available models to identify isolates that may provide a higher degree of pathogenesis in the relatively restricted hosts evaluated to date so that an improved model of this emerging viral pathogen can be developed.

Materials and methods

Virus and cells

MERS-CoV Jordan-n3/2012 was propagated in MRC-5 cells at a multiplicity of infection (MOI) of 0.1 for 5 days. MRC-5 cells were maintained in Eagle's Modified Essential medium (EMEM) (HyClone, Logan, UT) supplemented with 5% fetal bovine serum (FBS) (Sigma St. Louis MO) at 37 °C with 5% CO_2. MRC5 cells were maintained in EMEM supplemented with 10% FBS and 1% penicillin and streptomycin at 37 °C with 5% CO_2. Virus was recovered by removal of the tissue culture media followed by a low speed centrifugation, 500 g for 10 min at 4 °C to remove cellular debris stored at −80 °C, titered by limiting dilution plaque assays on Vero E6 cells (ATCC) and evaluated for mycoplasma and endotoxin contamination.

Monoclonal antibodies

The genes encoding 3B11 and 4E10 were expressed as IgG_1 using a viral-based transient expression system (magnICON) (Giritch et al., 2006) was used as the host plant for transient expression after infection with recombinant *Agrobacterium tumefaciens* (Strasser et al., 2008). The mAbs (3B11-N and 4E10-N) were purified as previously described (Zeitlin et al., 2013) to greater than 99% purity as assessed by SDS/PAGE and HPLC–size-exclusion chromatography.

Challenge and monitoring of NHPs

Twelve rhesus monkeys (*Macaca mulatta*), ranging in weight from 5.2 to 6.3 kg and 3–19 years old were screened prior to enrollment for simian retrovirus (SRV), simian T-lymphotrophic virus (STLV). The subjects were divided into five groups. Group 1 received γ-irradiated, proven inactivated virus, Group 2, 4 and 5 received 5×10^6 PFU of MERS-JOR, and Group 3 received 5×10^6 PFU of MERS-JOR and bronchoalveolar lavage. Inocula was performed with 2.5 mls of EMEM by placement of an endotracheal tube 4-5 cm above the carina followed by 2.5 ml s of PBS and air flush to ensure delivery of the inoculum. Groups 4 and 5 received 13 mg/kg of antibody by IV infusion. All animal procedures were performed at the National Institute of Allergy and Infectious Diseases Division of Clinical Research Integrated Research Facility and approved by the National Institute of Allergy and Infectious Diseases Division of Clinical Research Animal Care and Use Committee, and adhered to National Institutes of Health (NIH) policies.

Prior to and post inoculation, computed tomography (CT), physical exams, including temperature, weight, were performed, and blood draws and swabs from oral and nasal cavities were taken on days −18 to −14, 0, 3, 6, 9, 12, 15, 18, 21 and 28 days

post-inoculation. For Group 3 subjects, pediatric bronchoscope guided bronchoalveolar lavage was performed. Subjects were maintained on isoflurane during CT procedures. NHPs were monitored at least twice daily and euthanized when they met established endpoint criteria. A pre-established scale was used to evaluate subject health and disease progression, these criteria included: (1) overall clinical appearance, (2) labored breathing, (3) activity and behavior, (4), responsiveness, and (5) core body temperatures. No subjects met moribund clinical endpoint criteria. At days 91 and 93 post initial inoculation and (days 3 and 5 post third inoculation) NHPs were humanely euthanized. Blood, oral and nasal swabs were collected and select tissues were excised for virological and histopathological analysis as described below. Group 1 subjects were not euthanized.

Computed tomography (CT)

We acquired high resolution breath-hold chest CT data with a hybrid Philips Precedence 16P SPECT/CT scanner specifically designed to function in a BSL4 environment. We used 140 kVp at 300 mA s with a 160 mm axial field of view at a 0.8 mm slice thickness and 0.4 mm increment covering the whole lung. Reconstruction was performed on a 512 by 512 matrix using a Lung filter.

CT image analysis

For each individual subject, lung region of interest (ROI) was initially segmented and the normal lung parenchyma's volume was determined using fuzzy connectedness based image segmentation algorithm (Mansoor et al., 2014). Subsequently, a random-forest based machine-learning algorithm was applied for determining the volume and spatial extent of the pathological regions and added into the lung ROI. Mainly, ground glass opacities and consolidations were observed as pathological tissues; therefore, the machine-learning algorithm was tuned to optimally detect these abnormal imaging patterns apart from normal tissues. Once normal and all pathological tissues were identified, percent of the abnormal lung was computed through total pathological tissue volume divided by the total lung capacity. Airways and airway walls were also delineated using a graph-based segmentation algorithm (Xu et al., 2013) for exploring whether the infection reaches and affects the airways; however, we did not find significant volume or density changes either on airways or airway walls. Similar routine was used to evaluate candidate vaccine approaches in MERS-CoV (Wang et al., 2015).

Hematology and serology

Complete blood cell differential count (CBC/diff) was determined from blood samples collected in ethylenediaminetetraacetic acid (EDTA)-coated blood tubes and analyzed using a Sysmex XT2000V™ (Sysmex America, Mundelein, IL). Serum chemistry values were assayed using the Piccolo CMP panel.

Plaque assay

Plaque assays were performed on the tissue samples excised at necropsy. At necropsy tissues were flash frozen, and stored at −80 °C. A w/v homogenate between 10 and 30% was generated and serial 10 fold dilutions were made and incubated on confluent VeroE6 cells overlayed with 1.6% tragacanth. Following incubation, Tragacanth overlays were removed, the monolayers were stained with crystal violet (0.1% crystal violet, 20% ethanol 10% formalin v/v), and plaques were enumerated.

Histopathology and immunohistochemistry

Group 2 and 3 subjects were necropsied on days 91, and 93 post inoculation. Forty one tissues from all major organ systems were collected and fixed in 10% neutral buffered formalin. Following fixation in 10% NBF, tissues were trimmed into 5mm thick sections and placed in cassettes. The tissues were then dehydrated through a series of graded alcohols, cleared in an organic solvent, and infiltrated with molten paraggin by the Sakura Tissue Tek VIP tissue processor (Sakura, VIP 6-a1). After processing, the tissues were placed into molds and embedded in paraffin (McCormick, Paraplast Plus). The resulting blocks were sectioned at 4–6 μm using a rotary microtome and floated on a 48 °C water bath before being picked up on Superfrost Plus Gold slides (Fisher, 15-188-48). The sections were then baked for 20 min at 60 °C and a hematoxylin and eosin (H&E) stain was applied using the Leica automated staining system (Leica, ST5020). Stained slides were then examined via standard light microscopy. To detect MERS-CoV antigen, immunohistochemistry was performed using a rabbit polyclonal antiserum against MERS-CoV (1:1000) (Sino Biologicals) as a primary antibody for detection of antigen. Tissues from an uninfected control animal were used to validate all immunohistochemistry procedures. H&E sections were examined by light microscopy by the veterinary pathologists (LH).

Electron microscopy

For ultrastructural morphological investigations, collected BAL's were fixed in 2.5% glutaraldehyde (EM Sciences, Warrington, PA USA) in Millonig's Sodium Phopshate Buffer (Tousimis Research, Rockville, MD USA) for 72 h. The preserved cells were post-fixed in 1.0% osmium tetroxide (E.M. Sciences), en bloc stained with 2.0% uranyl acetate, dehydrated in a graded ethanol series up to 100%, and embedded in Spurr plastic resin (E.M. Sciences). Embedded blocks were sectioned using a Leica UC7 ultramicrotome (Leica), 60–80 nm ultra-thin sections were collected, mounted on 200 mesh copper grids, and contrasted with lead cirate. The grids were then examined and imaged using a FE G2 Tecnai transmission electron microscope operating at 80 kB (Tecnai).

Quantification of viremia by quantitative PCR

Viral load in samples was determined by quantitative PCR using the UpE assay as described by Corman et al. (2012). Samples were extracted with Trizol and screened for the presence of MERS-CoV using specific primers on an ABI 7900HT. The limit of detection was 100 gene copies.

Statistical analysis

To compare group differences for lung pathology, data from day 0 to day 14 was analyzed. A linear mixed model was used by taking the correlation within each subject into account (Laird and Ware, 1982). To reflect the possible nonlinear effect from days, we have used linear, quadratic, and cubic terms for day effect. Data analyses were performed in S-plus. Due to the multiple comparison problem, a more stringent P value of less than 0.01 will be claimed to be significant.

Acknowledgments

This work was supported by the NIAID Division of Intramural Research. We are grateful to Marisa St. Claire, Russell Byrum, Dan Ragland, and the entire EVPS and IRF team for their contributions to these studies. We thank Jiro Wada for his contribution to the preparation of figures. The content of this publication does not necessarily reflect the views or policies of the US Department of Health and Human Services (DHHS) or of the institutions and companies affiliated with the authors. This work was funded in part through Battelle Memorial Institute's prime contract with the US National Institute of Allergy and Infectious Diseases (NIAID) under Contract no. HHSN272200700016I. B.L.O., M.R.H., J.C.J. performed this work as employees of Battelle Memorial Institute. Subcontractors to Battelle Memorial Institute who performed this work are: E.P. an employee of Tunnell Government Services, Inc.; N.O., S.Y. and L.H. are employees of Charles River Laboratories, S.M. an employee of MRI Global, CB an employee of MedRelief. J.S. is an employee with Leidos. His part in the project has been funded in whole or in part with federal funds from the National Cancer Institute, National Institutes of Health, under Contract No. HHSN261200800001E. W.A.M. and R.S.B. were supported by Grant R01AI085524 from NIAID. W.A.M also received support from Defense Advanced Research Projects Agency Grant W911NF-10-0226. The authors thank Drs. Yuri Gleba and Victor Klimyuk (Icon Genetics) for access to the magnICON expression technology and Dr. Herta Steinkellner (BOKU) for access to the *N. benthamiana* seed.

Appendix A. Supplementary material

Supplementary data associated with this article can be found in the online version at http://dx.doi.org/10.1016/j.virol.2016.01.004.

References

Adney, D.R., van Doremalen, N., Brown, V.R., Bushmaker, T., Scott, D., de Wit, E., Bowen, R.A., Munster, V.J., 2014. Replication and shedding of MERS-CoV in upper respiratory tract of inoculated dromedary camels. Emerg. Infect. Dis. 20, 1999–2005.

Agrawal, A.S., Garron, T., Tao, X., Peng, B.H., Wakamiya, M., Chan, T.S., Couch, R.B., Tseng, C.T., 2015. Generation of a transgenic mouse model of Middle East respiratory syndrome coronavirus infection and disease. J. Virol. 89, 3659–3670.

Bossart, K.N., Zhu, Z., Middleton, D., Klippel, J., Crameri, G., Bingham, J., McEachern, J.A., Green, D., Hancock, T.J., Chan, Y.P., Hickey, A.C., Dimitrov, D.S., Wang, L.F., Broder, C.C., 2009. A neutralizing human monoclonal antibody protects against lethal disease in a new ferret model of acute nipah virus infection. PLoS Pathog. 5, e1000642.

Channappanavar, R., Fett, C., Zhao, J., Meyerholz, D.K., Perlman, S., 2014a. Virus-specific memory CD8 T cells provide substantial protection from lethal severe acute respiratory syndrome coronavirus infection. J. Virol. 88, 11034–11044.

Channappanavar, R., Zhao, J., Perlman, S., 2014b. T cell-mediated immune response to respiratory coronaviruses. Immunol. Res. 59, 118–128.

Corman VM1, Eckerle I, Bleicker T, Zaki A, Landt O, Eschbach-Bludau M, van Boheemen S, Gopal R, Ballhause M, Bestebroer TM, Muth D, Müller MA, Drexler JF, Zambon M, Osterhaus AD, Fouchier RM, Drosten C. 2012. Detection of a novel human coronavirus by real-time reverse-transcription polymerase chain reaction., Euro Surveillance 17(39).

de Groot, R.J., Baker, S.C., Baric, R.S., Brown, C.S., Drosten, C., Enjuanes, L., Fouchier, R.A., Galiano, M., Gorbalenya, A.E., Memish, Z.A., Perlman, S., Poon, L.L., Snijder, E.J., Stephens, G.M., Woo, P.C., Zaki, A.M., Zambon, M., Ziebuhr, J., 2013. Middle East respiratory syndrome coronavirus (MERS-CoV): announcement of the Coronavirus Study Group. J. Virol. 87, 7790–7792.

de Wit, E., Rasmussen, A.L., Falzarano, D., Bushmaker, T., Feldmann, F., Brining, D.L., Fischer, E.R., Martellaro, C., Okumura, A., Chang, J., Scott, D., Benecke, A.G., Katze, M.G., Feldmann, H., Munster, V.J., 2013. Middle East respiratory syndrome coronavirus (MERS-CoV) causes transient lower respiratory tract infection in rhesus macaques. Proc. Natl. Acad. Sci. USA 110, 16598–16603.

Falzarano, D., de Wit, E., Feldmann, F., Rasmussen, A.L., Okumura, A., Peng, X., Thomas, M.J., van Doremalen, N., Haddock, E., Nagy, L., LaCasse, R., Liu, T., Zhu, J., McLellan, J.S., Scott, D.P., Katze, M.G., Feldmann, H., Munster, V.J., 2014. Infection with MERS-CoV causes lethal pneumonia in the common marmoset. PLoS Pathog. 10, e1004250.

Giritch, A., Marillonnet, S., Engler, C., van Eldik, G., Botterman, J., Klimyuk, V., Gleba, Y., 2006. Rapid high-yield expression of full-size IgG antibodies in plants coinfected with noncompeting viral vectors. Proc. Natl. Acad. Sci. USA 103, 14701–14706.

Gossner, C., Danielson, N., Gervelmeyer, A., Berthe, F., Faye, B., Kaasik Aaslav, K., Adlhoch, C., Zeller, H., Penttinen, P., Coulombier, D., 2014. Human-dromedary camel interactions and the risk of acquiring zoonotic Middle East Respiratory syndrome coronavirus infection. Zoonoses Public Health.

Haley, P.J., Muggenburg, B.A., Rebar, A.H., Shopp, G.M., Bice, D.E., 1989. Bronchoalveolar lavage cytology in cynomolgus monkeys and identification of cytologic alterations following sequential saline lavage. Vet. Pathol. 26, 265–273.

Jiang, L., Wang, N., Zuo, T., Shi, X., Poon, K.M., Wu, Y., Gao, F., Li, D., Wang, R., Guo, J., Fu, L., Yuen, K.Y., Zheng, B.J., Wang, X., Zhang, L., 2014. Potent neutralization of MERS-CoV by human neutralizing monoclonal antibodies to the viral spike glycoprotein. Sci. Transl. Med. 6, 234ra259.

Johnson, R.F., Via, L.E., Kumar, M.R., Cornish, J.P., Yellayi, S., Huzella, L., Postnikova, E., Oberlander, N., Bartos, C., Ork, B.L., Mazur, S., Allan, C., Holbrook, M.R., Solomon, J., Johnson, J.C., Pickel, J., Hensley, L.E., Jahrling, P.B., 2015. Intratracheal exposure of common marmosets to MERS-CoV Jordan-n3/2012 or MERS-CoV EMC/2012 isolates does not result in lethal disease. Virology 485, 422–430.

Khalafalla, A.I., Lu, X., Al-Mubarak, A.I., Dalab, A.H., Al-Busadah, K.A., Erdman, D.D., 2015. MERS-CoV in Upper respiratory tract and lungs of dromedary camels, Saudi Arabia, 2013-2014. Emerg. Infect. Dis. 21, 1153–1158.

Laird, N.M., Ware, J.H., 1982. Random-effects models for longitudinal data. Biometrics 38, 963–974.

Mansoor, A., Bagci, U., Xu, Z., Foster, B., Olivier, K.N., Elinoff, J.M., Suffredini, A.F., Udupa, J.K., Mollura, D.J., 2014. A generic approach to pathological lung segmentation. IEEE Trans. Med. Imaging 33, 2293–2310.

Marasco, W.A., Sui, J., 2007. The growth and potential of human antiviral monoclonal antibody therapeutics. Nat. Biotechnol. 25, 1421–1434.

Munster, V.J., de Wit, E., Feldmann, H., 2013. Pneumonia from human coronavirus in a macaque model. N Engl. J. Med. 368, 1560–1562.

Pascal, K.E., Coleman, C.M., Mujica, A.O., Kamat, V., Badithe, A., Fairhurst, J., Hunt, C., Strein, J., Berrebi, A., Sisk, J.M., Matthews, K.L., Babb, R., Chen, G., Lai, K.M., Huang, T.T., Olson, W., Yancopoulos, G.D., Stahl, N., Frieman, M.B., Kyratsous, C. A., 2015. Pre- and postexposure efficacy of fully human antibodies against Spike protein in a novel humanized mouse model of MERS-CoV infection. Proc. Natl. Acad. Sci. USA 112, 8738–8743.

Pebody, R.G., Chand, M.A., Thomas, H.L., Green, H.K., Boddington, N.L., Carvalho, C., Brown, C.S., Anderson, S.R., Rooney, C., Crawley-Boevey, E., Irwin, D.J., Aarons, E., Tong, C., Newsholme, W., Price, N., Langrish, C., Tucker, D., Zhao, H., Phin, N., Crofts, J., Bermingham, A., Gilgunn-Jones, E., Brown, K.E., Evans, B., Catchpole, M., Watson, J.M., 2012. The United Kingdom public health response to an imported laboratory confirmed case of a novel coronavirus in September 2012. Euro Surveill.: Bull. Eur. sur Les Mal. Transm. Eur. Commun. Dis. Bull. 17, 8–11.

Qiu, X., Kobinger, G.P., 2014. Antibody therapy for Ebola: is the tide turning around? Hum. Vaccines Immunother. 10, 964–967.

Raj, V.S., Mou, H., Smits, S.L., Dekkers, D.H., Muller, M.A., Dijkman, R., Muth, D., Demmers, J.A., Zaki, A., Fouchier, R.A., Thiel, V., Drosten, C., Rottier, P.J., Osterhaus, A.D., Bosch, B.J., Haagmans, B.L., 2013. Dipeptidyl peptidase 4 is a functional receptor for the emerging human coronavirus-EMC. Nature 495, 251–254.

Shadman, K.A., Wald, E.R., 2011. A review of palivizumab and emerging therapies for respiratory syncytial virus. Expert. Opin. Biol. Ther. 11, 1455–1467.

Strasser, R., Stadlmann, J., Schahs, M., Stiegler, G., Quendler, H., Mach, L., Glossl, J., Weterings, K., Pabst, M., Steinkellner, H., 2008. Generation of glyco-engineered Nicotiana benthamiana for the production of monoclonal antibodies with a homogeneous human-like N-glycan structure. Plant Biotechnol. J. 6, 392–402.

Tang, X.C., Agnihothram, S.S., Jiao, Y., Stanhope, J., Graham, R.L., Peterson, E.C., Avnir, Y., Tallarico, A.S., Sheehan, J., Zhu, Q., Baric, R.S., Marasco, W.A., 2014. Identification of human neutralizing antibodies against MERS-CoV and their role in virus adaptive evolution. Proc. Natl. Acad. Sci. USA 111, E2018–E2026.

Von Essen, S.G., Robbins, R.A., Spurzem, J.R., Thompson, A.B., McGranaghan, S.S., Rennard, S.I., 1991. Bronchoscopy with bronchoalveolar lavage causes neutrophil recruitment to the lower respiratory tract. Am. Rev. Respir. Dis. 144, 848–854.

Wang, L., Shi, W., Joyce, M.G., Modjarrad, K., Zhang, Y., Leung, K., Lees, C.R., Zhou, T., Yassine, H.M., Kanekiyo, M., Yang, Z.Y., Chen, X., Becker, M.M., Freeman, M., Vogel, L., Johnson, J.C., Olinger, G., Todd, J.P., Bagci, U., Solomon, J., Mollura, D.J., Hensley, L., Jahrling, P., Denison, M.R., Rao, S.S., Subbarao, K., Kwong, P.D., Mascola, J.R., Kong, W.P., Graham, B.S., 2015. Evaluation of candidate vaccine approaches for MERS-CoV. Nat. Commun. 6, 7712.

Xu Z., Bagci U., Foster B., Mansoor A., Mollura D.J., 2013. Spatially constrained random walk approach for accurate estimation of airway wall surfaces. Medical image computing and computer-assisted intervention: MICCAI International Conference on Medical Image Computing and Computer-Assisted Intervention, 16. p. 559–66.

Yao, Y., Bao, L., Deng, W., Xu, L., Li, F., Lv, Q., Yu, P., Chen, T., Xu, Y., Zhu, H., Yuan, J., Gu, S., Wei, Q., Chen, H., Yuen, K.Y., Qin, C., 2014. An animal model of MERS produced by infection of rhesus macaques with MERS coronavirus. J. Infect. Dis. 209, 236–242.

Ying, T., Li, H., Lu, L., Dimitrov, D.S., Jiang, S., 2015. Development of human neutralizing monoclonal antibodies for prevention and therapy of MERS-CoV infections. Microbes Infect. 17, 142–148, institut Pasteur.

Yusof, M.F., Eltahir, Y.M., Serhan, W.S., Hashem, F.M., Elsayed, E.A., Marzoug, B.A., Abdelazim, A.S., Bensalah, O.K., Al Muhairi, S.S., 2015. Prevalence of Middle East

respiratory syndrome coronavirus (MERS-CoV) in dromedary camels in Abu Dhabi Emirate, United Arab Emirates. Virus Genes 50, 509–513.
Zaki, A.M., van Boheemen, S., Bestebroer, T.M., Osterhaus, A.D., Fouchier, R.A., 2012. Isolation of a novel coronavirus from a man with pneumonia in Saudi Arabia. N Engl. J. Med. 367, 1814–1820.
Zeitlin, L., Bohorov, O., Bohorova, N., Hiatt, A., Kim do, H., Pauly, M.H., Velasco, J., Whaley, K.J., Barnard, D.L., Bates, J.T., Crowe Jr., J.E., Piedra, P.A., Gilbert, B.E., 2013. Prophylactic and therapeutic testing of Nicotiana-derived RSV-neutralizing human monoclonal antibodies in the cotton rat model. mAbs 5, 263–269.
Zhao, J., Li, K., Wohlford-Lenane, C., Agnihothram, S.S., Fett, C., Zhao, J., Gale Jr., M.J., Baric, R.S., Enjuanes, L., Gallagher, T., McCray Jr., P.B., Perlman, S., 2014. Rapid generation of a mouse model for Middle East respiratory syndrome. Proc. Natl. Acad. Sci. USA 111, 4970–4975.
Zwick, M.B., Labrijn, A.F., Wang, M., Spenlehauer, C., Saphire, E.O., Binley, J.M., Moore, J.P., Stiegler, G., Katinger, H., Burton, D.R., Parren, P.W., 2001. Broadly neutralizing antibodies targeted to the membrane-proximal external region of human immunodeficiency virus type 1 glycoprotein gp41. J. Virol. 75, 10892–10905.